Oceanologia (2018) 60, 76—85

Available online at www.sciencedirect.com

ScienceDirect

journal homepage: www.journals.elsevier.com/oceanologia/

ORIGINAL RESEARCH ARTICLE

Spatio-temporal variability in the Brazil-Malvinas Confluence Zone (BMCZ), based on spectroradiometric MODIS-AQUA chlorophyll-*a* observations

Luciano Telesca [a,*], **Jorge O. Pierini** [b], **Michele Lovallo** [c], **Eduardo Santamaría-del-Angel** [d]

[a] *National Research Council, Institute of Methodologies for Environmental Analysis, Tito, PZ, Italy*
[b] *Comisión de Investigaciones Científicas (CIC) — IADO-CONICET, Bahía Blanca, Argentina*
[c] *ARPAB, Potenza, Italy*
[d] *Universidad Autónoma de Baja California, Baja California, Mexico*

Received 28 March 2017; accepted 7 August 2017
Available online 26 August 2017

KEYWORDS
MODIS;
Ocean color spectroradiometric chlorophyll-*a*;
Remote sensing oceanography;
Statistics

Summary The Brazil—Malvinas Confluence Zone (BMCZ) is characterized by high environmental variation, which could be reflected in several optical types of water, from one containing only phytoplankton and sea water to other optically more complex. In this paper, we analyze the spatio-temporal variability of the Chlorophyll-*a* detected by the ocean color sensor ($CHLA_{sat}$) in BMCZ in order to understand its environmental variability. We use the MODIS-Aqua $CHLA_{sat}$ monthly composites imagery from 2002 to 2015, and applied two statistical methods: the correlogram-based robust periodogram to identify, over a broad spectrum of temporal, the most significant periodicities, and the pixel gradient distribution to study the spatial-temporal gradients within the BMCZ and variations over the continental shelf and coastal waters. Our results point out to the predominance of the annual cycle over most of the investigated area, although an area from latitude 37°S in direction NE, alongshore of Uruguay to Brazil, evidences interannual periodicities, possibly related to variations in the discharge of the Rio de la Plata associated with the El Niño phenomena. The ocean color spectroradiometric signature in terms of

* Corresponding author at: C.da S. Loja, 85050 Tito, PZ, Italy. Tel.: +39 0971427277; fax: +39 0971427271.
E-mail address: luciano.telesca@imaa.cnr.it (L. Telesca).

Peer review under the responsibility of Institute of Oceanology of the Polish Academy of Sciences.

ELSEVIER Production and hosting by Elsevier

http://dx.doi.org/10.1016/j.oceano.2017.08.002

pixel gradient presents a relatively high variability (~0.0 to 0.65 mg m^{-3}); in particular the high values of the pixel gradient correspond to saline front of the estuarine system of Rio de la Plata, and to the strip of the platform that extends along the isobaths of 80 m (coast of Uruguay), especially in the center and south of the study area.

1. Introduction

Ocean fronts over continental shelf are closely linked to bathymetric features. Besides these, other important fronts are associated with the discharge of large rivers: Rio de la Plata, for instance, represents a clear example over our study area (Brazil-Malvinas Confluence Zone). The discharge of this river is one of the largest in the southern hemisphere and the second largest after that of the Amazon River, contributing to an average of about 24,000 $m^3 s^{-1}$ of fresh nutrient-rich water of the Atlantic Ocean. Furthermore, seasonal rainfalls, especially intense during El Niño periods, contribute to increase the discharge of Rio de la Plata up to about 80,000 $m^3 s^{-1}$ (Acha et al., 2004; Depetris and Kempe, 1990; Guerrero et al., 1997; Huret et al., 2005; Mechoso and Iribarren, 1992). The fresh water plume travels over the continental shelf mainly responding to the bottom topography and seasonal characteristics of the main winds and can extend its influence to northern Uruguay – South Brazil or move south until reaching Mar del Plata city (Braga et al., 2008). The ocean waters are also influenced by contributions from warm waters of subtropical origin (Brazil Current) and cold waters of subantarctic origin (Malvinas current). These two water masses converge on the edge of the continental shelf, creating what is known as the Brazil-Malvinas confluence (BMCZ) (Gordon, 1989).

This region contrasts with the low phytoplankton concentrations of the Brazilian current (nutrient scarcity affects the growth of the primary producers) and the Malvinas current, although they are rich in nutrients, due to the presence of permanent winds, these vertically mix the water column and prevent the production of phytoplankton. Phytoplankton accumulation is observed only along narrow strips on the ocean surface, and its productivity is due to the fact that both currents provide elements that favor their growth and concentration. If the Malvinas Current brings nutrient-rich water, the Brazil Current makes phytoplankton growth quite stable and thanks to such stability of subtropical warm waters, the growth of phytoplankton is very significant (Carreto et al., 1995; Romero et al., 2006).

The frontal areas coincide with the geographical location of phytoplankton blooms. Marine phytoplankton abundance and productivity are subject to complex set of relationships between physical and biological patterns that appear to be different in physically distinct regions. Several ocean studies, in which ocean color satellite images were used, have shown high chlorophyll-*a* concentration structures in the BMCZ (Piola et al., 2000), but on the other hand, still few studies have been carried out on its space-time variability in such important area of the confluence (Machado et al., 2013).

The availability of remote sensing technology has enabled the identification of physical and biological synoptic patterns over the BMCZ. Most studies have been based on the analysis of the seasonal variability of in situ Chlorophyll-*a*, while the interannual variability remains still less approached due to the relatively short length of time series (Garcia and Garcia, 2008; Lutz et al., 2010; Machado et al., 2013; Romero et al., 2006).

Changes in ecosystems have already been reported by other authors, and the abrupt and nonlinear potential can again be more likely future changes (Machado et al., 2013). To understand these changes in marine ecosystems, with essential data sets with lots of information, thus, the satellite ocean color data are valuable assets. The global coverage provided by satellites provides a long time series of records of concentration of Chlorophyll-*a* detected by ocean color sensor ($CHLA_{sat}$), which is especially suited to identify patterns of temporal variability (Brandini et al., 2000; Piola et al., 2008), not only of phytoplankton biomass but also of all the optical components present in seawater, which absorb the same wavelengths as chlorophyll in optical complex water.

Argentina's continental shelf is a highly productive area; with values of phytoplankton abundance around three times the average for the rest of the oceans. Phytoplankton find not evenly distributed, but has a higher concentration in certain regions associated with ocean fronts (Marrari et al., 2016). In our study, we aim at describing quantitatively the temporal variations of the $CHLA_{sat}$ in the BMCZ by using two statistical approaches the robust periodogram and the pixel gradient distribution, never used to investigate the variability of the $CHLA_{sat}$, up to our knowledge.

2. Data analysis

The satellite data we used in our study are provided by the polar orbiting satellite AQUA, which carries the Moderate Resolution Imaging Spectrophotometer (MODIS). AQUA has a sun-synchronous circular orbit, overpasses any given location on Earth twice a day (one night time and one day time pass) and it orbits the Earth every 98.8 min, crossing the equator from south to north each day. Modis Aqua imagery were building at level 3 GLO (4 km resolution) in the Ocean color laboratory in the Facultad de Ciencias Marinas (Universidad Autonoma de Baja California). The level 1b data were obtained from the NASA Ocean Color Data web page (http://oceandata.sci.gsfc.nasa.gov/). The level 1b to level 2 conversion was made carried out using the SEADAS 6 using the specifically atmospherically data form each scene. The level 2 to level 3 monthly GLO imagery processing was made

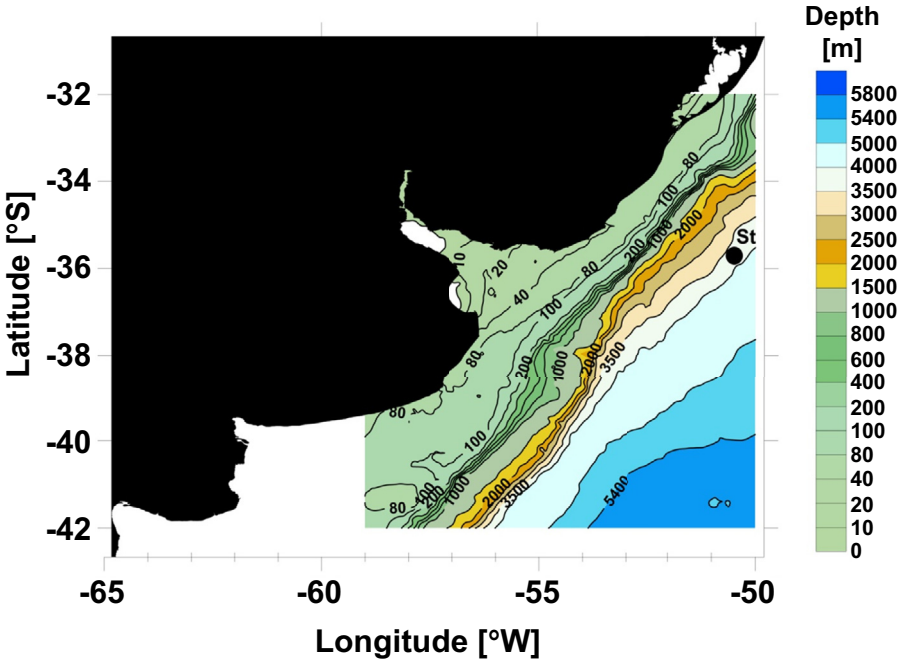

Figure 1 The BMCZ. The black circle St marks the pixel whose time variation is plotted in Fig. 2.

using a WIM software (http://wimsoft.com/) with the WIM automation Module (WAM) ver. 9.10.

The area of interest extends from 50°W to 60°W and from 32°S to 42°S including the BMCZ (Fig. 1). We used the monthly MODIS AQUA images from July 2002 to April 2015; the length of each pixel time series is 154.

Before analyzing the time variation of each pixel in the area (Fig. 1), we pre-processed the data to remove outliers. Fig. 2a shows, as an example, the time variation of $CHLA_{sat}$ corresponding to the pixel (Lat = −35.945833, Lon = −50.8087963), and it is clearly visible the presence of outliers. We applied a third-order one-dimensional median filter to the data and removed all the values whose absolute difference from the filtered signal is above 1. Fig. 2b shows the same time series plotted in Fig. 2a but with the outliers removed ($CHLA_{s,f}$).

Fig. 3 shows the mean $CHLA_{s,f}$ only for pixel time series longer than 50 samples. The data suggest a high concentration of mean $CHLA_{s,f}$ in the nearshore region, alongshore of Uruguay, that reflect the longitudinal gradients within these coastal waters. Such high concentration does not mean a real increase in chlorophyll, but it may be a response to the pulses of sediment and other substances that drag the river during discharges or by the waves, forced by storms, that could generate sediments resuspension favoring the vertical mixture.

For each filtered pixel, we computed the standardized anomaly $CHLA_d = (CHLA_{s,f} - \langle CHLA_{s,f}\rangle)/std(CHLA_{s,f})$, where the $\langle CHLA_{s,f}\rangle$ is the calendar mean, that is calculated for each calendar month, *e.g.* January, by averaging over all years in the record (Pierini et al., 2016) and $std(CHLA_{s,f})$ is the calendar standard deviation. Fig. 4 shows the anomaly $CHLA_d$ for the same pixels shown in Fig. 2.

The most of pixel time series present from low to high percentage of missing data; since the size of the time series is rather small, the presence of missing data reduces further such size, preventing us calculating the power spectral density by using the classical Fourier Transform. For this reason, we used a recently developed algorithm based on the correlogram to robustly calculate the periodogram and, therefore, obtain information about the spectral content of the $CHLA_d$ time series and identify their most significant periodicity. Furthermore, we applied the pixel gradient distribution analysis to evaluate the spatial-temporal gradients within the study region and the variations over continental shelf and coastal waters.

2.1. Robust periodogram method

Among the several complex features a natural phenomenon is characterized by, the robust identification of periodicities are the first type of time fluctuations that are necessary to be detected and investigated. Observational data are generally affected by noise, gaps, spikes; furthermore they could also be very short, making crucial the use of efficient algorithms to obtain as much information as possible.

Wichert et al. (2004) introduced a formal statistical testing procedure for the detection of periodicities, based on the so-called Fisher's g-statistic for which the exact null-distribution can be derived under the Gaussian noise assumption. Considering the following simple model of periodic series:

$$y_n = \beta\cos(\omega t + \phi) + \epsilon_n, \tag{1}$$

where $\beta > 0$, $0 < \omega < \pi$, ϕ uniformly distributed in $(-\pi, \pi]$, and $\{\varepsilon_n\}$ is a sequence of uncorrelated random variables with mean 0 and variance σ^2, independent of ϕ.

Then, the classical periodogram is given by the following formula:

$$I(\omega) = \frac{1}{N}\left|\sum_{n=1}^{N} y_n e^{-i\omega n}\right|^2, \quad 0 \le \omega \le \pi \tag{2}$$

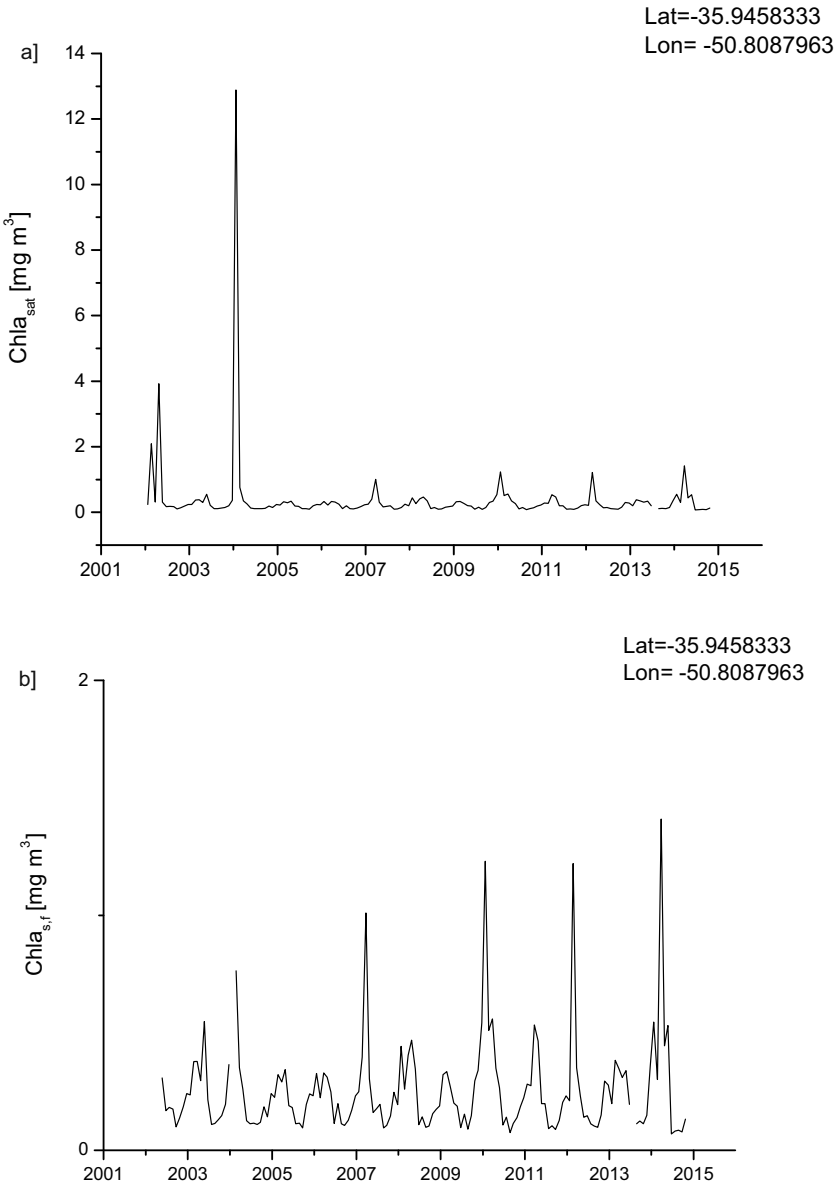

Figure 2 Time variation of $CHLA_{sat}$ (a) and $CHLA_{s,f}$ (b) corresponding to the pixel (Lat = −35.945833, Lon = −50.8087963).

where N is the length of the time series. The periodogram is further evaluated at normalized frequencies

$$\omega_l = \frac{2\pi l}{N}, \quad l = 0, 1, \ldots, a \tag{3}$$

where $a = [(N-1)/2]$ and $[x]$ indicates the integer part of x. If the signal has a significant cycle with frequency ω_0, then the periodogram has a high probability to exhibit a peak centered at that frequency. While, if the time series is a purely random process, which means $\beta = 0$ in Eq. (1), then the periodogram is uniform appearing flat for any frequency bands (Priestley, 1981).

The main periodicity (as argued by the highest peak in the periodogram) can be tested by using the g-statistics (Ahdesmäki et al., 2005):

$$g = \frac{\max_{1\le l\le a} I(\omega_l)}{\sum_{l=1}^{a} I(\omega_l)}, \tag{4}$$

which is the maximum periodogram ordinate divided by the sum of all periodogram ordinates for $l = 1, \ldots, a$. Large value of g indicates strong periodicity and leads to the rejection of the null hypothesis.

Wichert et al. (2004) calculated the exact p-value for a realization of the g-statistics, under the Gaussian noise assumption:

$$P(g > x) = a(1-x)^{a-1} - \frac{a(a-1)}{2}(1-2x)^{a-1} + \cdots + (-1)^b \frac{a!}{b!(a-b)!}(1-bx)^{a-1}, \tag{5}$$

where b is the largest integer less than $1/x$ and x is the observed value of the g-statistic. Eq. (5), then, provides the exact significance value for a realization of the g-statistic under the assumption of Gaussian distribution of the noise.

Ahdesmäki et al. (2005) developed a robust detection of periodic time series based on the estimation of the

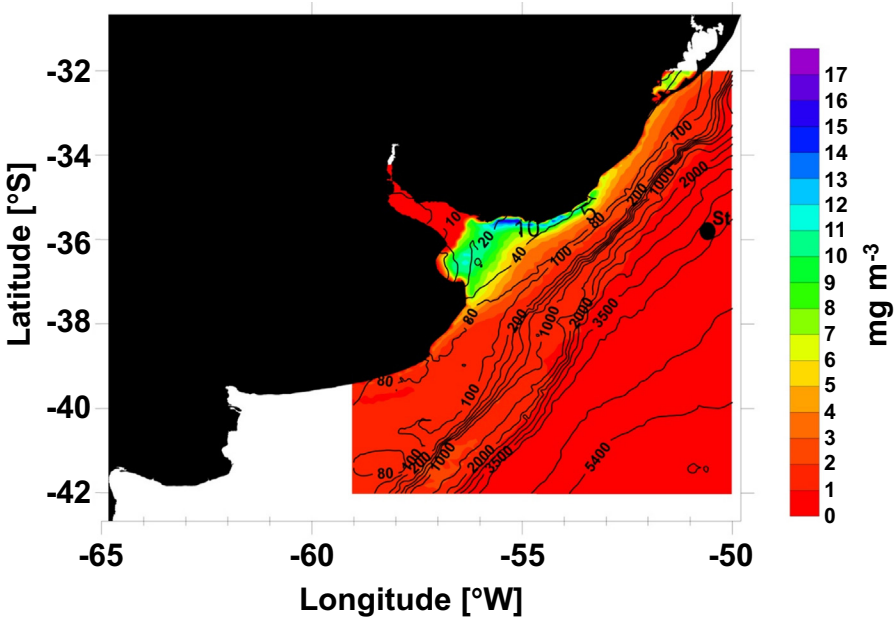

Figure 3 Spatial distribution of the mean $CHLA_{s,f}$. The black circle St marks the pixel whose time variation is plotted in Fig. 2.

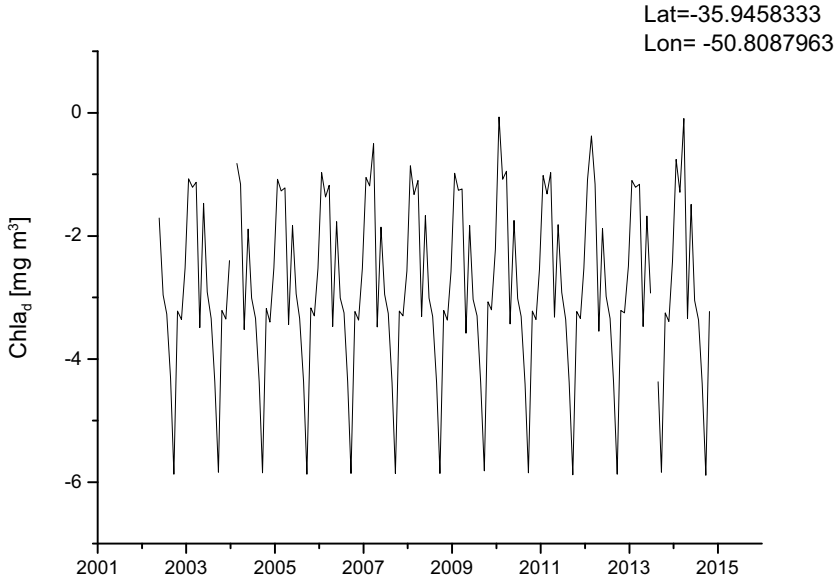

Figure 4 Standardized anomaly $CHLA_d$ for the same pixel shown in Fig. 2.

autocorrelation function. Since the periodogram $I(\omega)$ is equivalent to the correlogram spectral estimator

$$S(\omega) = \sum_{k=-N+1}^{N-1} \hat{r}(k) e^{-i\omega k}, \tag{6}$$

where

$$\hat{r}(m) = \frac{1}{N} \sum_{k=1}^{N-m} y_k y_{k+m} \tag{7}$$

is the biased estimator of the autocorrelation function, the g-statistics in Eq. (5) and the significance test in Eq. (6) can be calculated using $S(\omega)$ instead of $I(\omega)$. Recalling that the sample correlation function between two sequence with length N is given by

$$\rho(m) = \frac{\frac{1}{N}\sum_{i=1}^{N}(x_i - \overline{x})(y_i - \overline{y})}{\sigma_x \sigma_y}, \tag{8}$$

where the bar over the symbol indicates the mean; Ahdesmäki et al. (2005) obtained the following robust spectral estimator on the base of the relationship between the estimator of the autocorrelation function $\hat{r}(m)$ and the estimator of correlation function $\tilde{\rho}(m)$ between the sequences $\{y_k\}$ and $\{y_{k+m}\}$:

$$\tilde{S}(\omega) = 2\Re\left(\sum_{k=0}^{L}\tilde{\rho}(k)e^{-i\omega k}\right) - \tilde{\rho}(0), \quad (9)$$

where $\Re(x)$ indicates the real part of x, L is the maximum lag for which the correlation coefficient $\tilde{\rho}(k)$ is computed.

The g-statistics test can be modified as follows to test the significance of any frequency ω:

$$g = \frac{|\tilde{S}(\omega_l)|}{\sum_{l=1}^{a}|\tilde{S}(\omega_l)|}. \quad (10)$$

The significance values can be computed with the simulation-based method (Ahdesmäki et al., 2005): given the model as in Eq. (1) a set of P random time series are generated under the null hypothesis. The test statistics shown in Eq. (10) is evaluated for each index on each of the P time series. The obtained g-values are used to estimate the distribution of g-statistics under the null hypothesis and, therefore, the p-value.

Fig. 5 shows, as an example, the robust periodogram (Fig. 5a) of $CHLA_d$ time series corresponding to the pixel (Lat = −35.945833, Lon = −50.8087963) (Station 10001) and the p-value (Fig. 5b). The lowest p-value corresponds to the periodicity of about 12 months, which is the most significant.

For each pixel we calculated the robust periodogram and identified the most significant periodicity (the one corresponding to the lowest p-value). Since several pixel time series present data missings, we computed the robust periodogram only for those pixel time series whose amount of data missing is lower than 2/3 of the total length of the time series. Furthermore, we considered valid only those significant periodicities whose value was smaller than half of the overall period of the time series, thus only periodicities less than 77 months.

Fig. 6 shows the spatial variation of the most significant periodicity of $CHLA_d$. It is visible that relatively short period oscillations (up to 24 months) are spread almost all over the investigated area. However, predominant frequencies of relatively long period (above 24 months) extend around from latitude 37°S and longitude 56°W in direction NE, alongshore of Uruguay, where the impingement is on interannual temporal scales and variability slides along the bathymetry until Brazil.

2.2. Pixel gradient distribution

We investigated the mean $CHLA_d$ gradient distribution. For each pixel, at a specified time, the gradient magnitude is calculated using centered differences as (Saraceno et al., 2005):

$$\|grad(CHLA_d(i))\| = \sqrt{\left(\frac{CHLA_d(ix+1) - CHLA_d(ix-1)}{dist(ix+1, ix-1)}\right)^2 + \left(\frac{CHLA_d(iy+1) - CHLA_d(iy-1)}{dist(iy+1, iy-1)}\right)^2}, \quad (11)$$

where $(ix - 1)$ and $(ix + 1)$ are the neighbors of the ith pixel in the X (analogously in Y) direction; $dist$ is the distance in the X (analogously in Y) direction. Then, the time average of all the gradients for each pixel is calculated and the mean gradient distribution of $CHLA_d$ is computed only if the number of quadruples (two neighbors of ith pixel in X direction and two in Y direction, as indicated in formula (11)) is above 50 (Fig. 7). The pixel gradient distribution of $CHLA_d$ mainly varies between ∼0.0 and ∼0.65 mg m^{-3}. The influence of highly turbid waters of Río de La Plata can be clearly seen in the MODIS in Fig. 7. The highest chlorophyll gradient is found

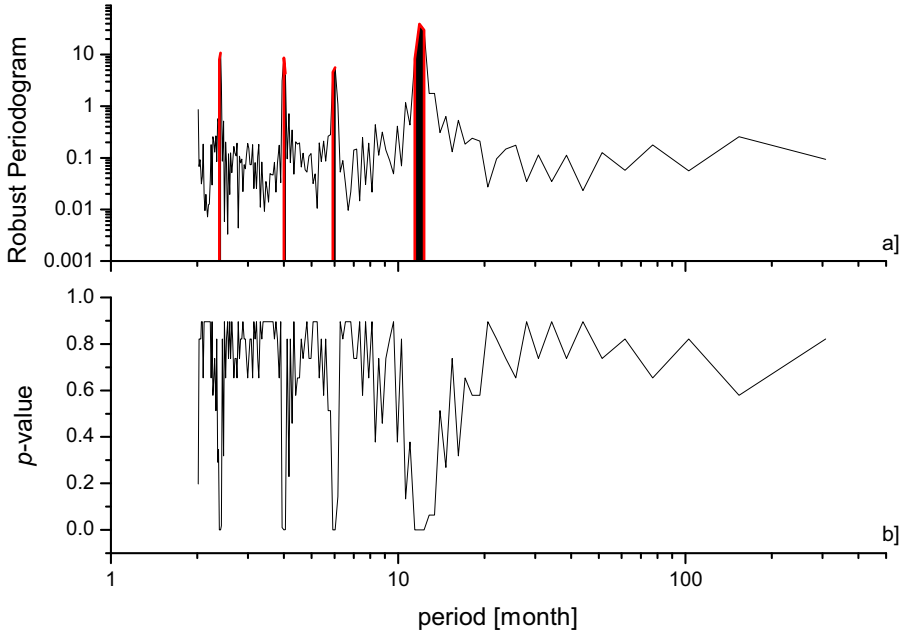

Figure 5 Robust periodogram of $CHLA_d$ time series corresponding to the pixel (Lat = −35.945833, Lon = −50.8087963) (a) and its p-value (b). The bold red part of the robust periodogram correspond to the frequencies that are significant with $p < 0.001$: the annual cycle and its higher harmonics (6 months, 4 months, 2.4 months) are clearly identified. (For interpretation of the references to color in this figure legend, the reader is referred to the web version of this article.)

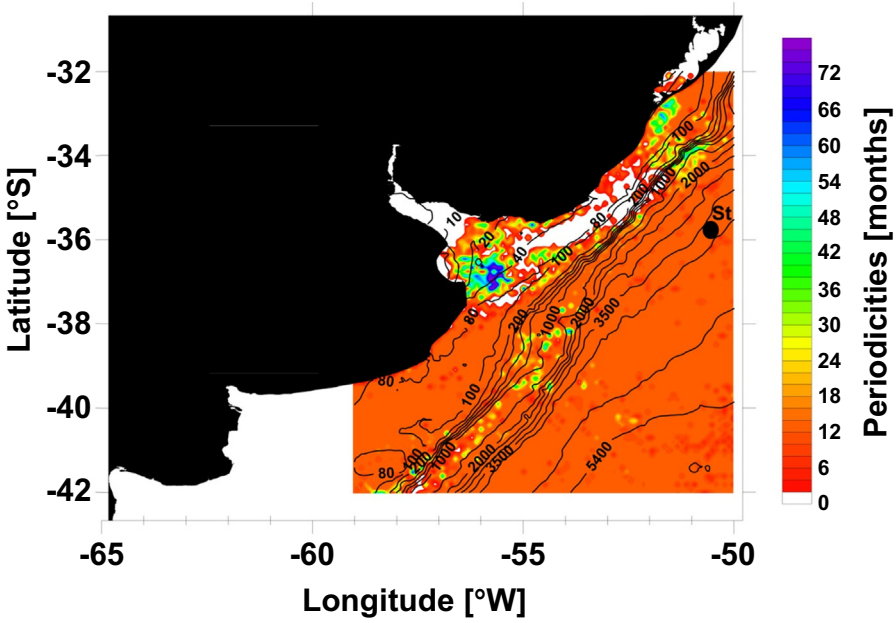

Figure 6 Spatial distribution of the most significant periodicity (months) of $CHLA_d$. The black circle St marks the pixel whose time variation is plotted in Fig. 2.

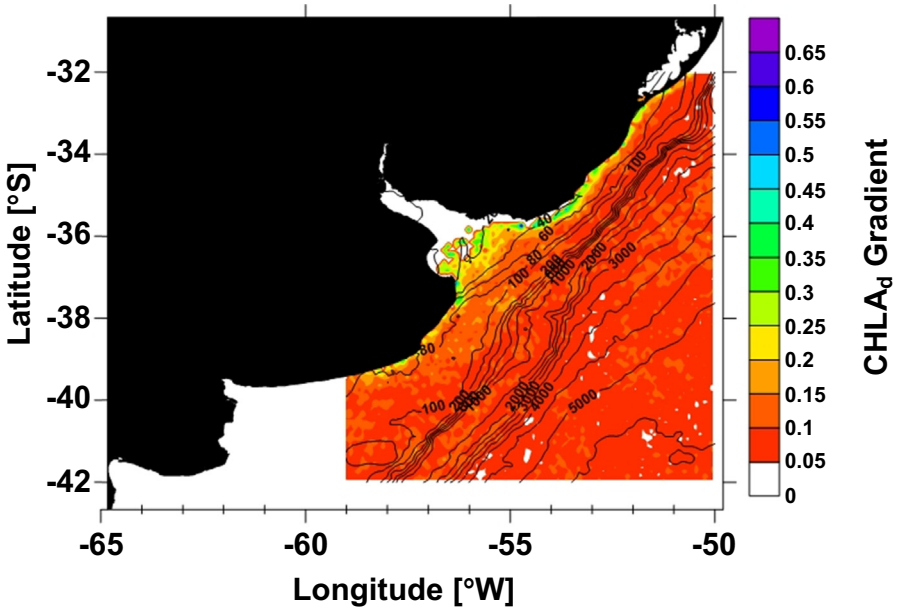

Figure 7 Pixel $CHLA_d$ gradient distribution.

near coastal regions. The pixel gradient map shows a spatial distribution of chlorophyll consistent with known patterns and expected values in the outer region of the Rio de la Plata. In fact, the highest gradient values can be observed along the northern tip of Samborombón Bay and the 15 and 45 m isobaths along south-north direction, showing a north-eastward discharge along the Uruguayan coast as also found by Calliari and Gomez (2005), Romero et al. (2006) and Simionato et al. (2004). The fluvial and estuarine domains in the West and the Oceanic domains in the East are divided by the thermohaline front, near isobaths 45 m along south-north direction. The discharge of the Río de la Plata registers low values of $CHLA_d$ due to the unfavorable conditions for the development of phytoplankton related to the low availability of light, being within the limit of salt intrusion (maximum turbidity); however a clear relationship with the gradient that measures the relative space-time variation of $CHLA_d$ cannot be established, due to the gaps in the time series of the pixels of that area (white zones in Fig. 7). In addition, a high gradient region is observed

near the coast and outer shelf area between 40° and 34°S, where, in addition, Malvinas slope water intrusion plays an important role in phytoplankton blooms (Piola et al., 2010; Romero et al., 2006).

3. Discussion

It is well known that at the mouth of Rio de la Plata estuarine highly variable, complex and unpredictable ecosystems exist (Day et al., 1989), where different forcing interact with geomorphologic configuration, depth, dimension of the estuary. Around the 30 m isobath, the chlorophyll variability is influenced mostly by local scale processes, such as river and estuarine outflow, wave effects, and nearshore circulation (Campos et al., 1999; Simionato et al., 2004, 2005). Nearshore coastal areas tend to exhibit high CHLA levels due to increased nutrient inputs from land runoff, riverine and estuarine flux, resuspension of sediments, pore water nutrients and recycling of nutrients. Nutrient loads of terrestrial origin to the nearshore waters of the Rio de la Plata increased by an order of magnitude (Martinez and Ortega, 2015). This is most likely due to the increase urbanization and agricultural use in the watersheds of the study area. These large freshwater flows can also set up salinity fronts, which may have the ability to inhibit the cross-shelf exchange of dissolved and suspended materials (Acha et al., 2004), thereby affecting the residence time of nutrients and phytoplankton growth limited by light availability on the inner shelf (Martinez and Ortega, 2015).

Several heterogeneous factors contribute to determine the high spatial-temporal variability of chlorophyll. The Rio de la Plata estuary, in fact, is of large scale type, characterized by large freshwater discharge; it also represents a very important area in the Argentine Platform Continental Shelf, featured by biophysical and biogeochemical processes related to the complex pattern of regional variability (Calliari and Gomez, 2005; Garcia and Garcia, 2008). These processes are mainly characterized by a strong annual cycle in most of the study area, although an area from latitude 37°S in direction NE, alongshore of Uruguay to Brazil, interannual periodicities are also evidenced (Fig. 6). Such periodicities may be the effect of variations in the discharge of the Rio de la Plata mainly associated with the El Niño phenomena, characterized by episodic hydro-meteorological phenomena (pulsatile) whose extreme manifestation are the floods, that cause significant impacts on the population (Acha et al., 2008; Depetris et al., 1996; Mechoso and Iribarren, 1992), that along with other external factors (wind, etc.) can introduce unstable conditions on CHLA (Gonzalez-Silvera et al., 2006; Piola et al., 2005; Sathicq et al., 2015).

The chlorophyll gradients presents a relatively high variability from 0.02 to 0.65 mg m^{-3}. The high values, indicating regions of high concentration, are assumed on two areas, isolated from each other. These two areas of increased phytoplankton abundance correspond to: (a) the saline front of the estuarine system of Rio de la Plata, and to (b) the strip of the platform that extends along the isobaths of 80 m (coast of Uruguay), especially in the center and south of the study area, which also occupies sectors of the intermediate platform sector (Acha et al., 2004). The results of the analysis of chlorophyll gradients suggest that this variable is closely linked with hydrodynamics processes. Indeed, at the mouth of the Rio de la Plata a marked increase gradient of chlorophyll can be seen, probably linked with the temperature and the amount of light hours (Framiñan and Brown, 1986). This phenomenon is expected considering that there abundant nitrogen and water clarity are enhanced by the sedimentation of particles in suspension, allowing penetration of light (Calliari and Gomez, 2005; Lasta et al., 1996). Chlorophyll gradients increase along the Uruguay coast of the Rio de la Plata and decrease outside along the coast of Argentina (Nagy et al., 1987). This could be correlated with the average displacement of fresh water plume in response to external forcings (wind, geometry depth, etc.). In the frontal domain (frontal region and marine adjacent zone) CHLA gradients are distributed as spots reaching maximum values of 0.65 mg m^{-3}. Rather high values of CHLA gradients are observed over the Samborombón Bay (37°S and 57°W), due to the geometry of the area. In the center and south of the deepest region of the platform sector, the CHLA gradient is less than that observed in the saline front at the mouth of the Rio de la Plata ($<$0.2 mg m^{-3}) and shows a more homogeneous spatial distribution.

4. Conclusions

By using the monthly AQUA MODIS satellite images from July 2002 to April 2015 we analyzed the spatial and temporal variability of CHLA data in the Brazil–Malvinas Confluence Zone, which represents one of the most productive oceanic areas worldwide. The spatial distribution of the average of CHLA over the investigated area indicates a high concentration in the nearshore region reflecting the longitudinal gradients within these coastal waters. Due to the short length of each pixel time series (only 154 values) that become even shorter in presence of missing data, we used a robust method for the identification of the most significant periodicities over the investigated area. A predominance of the annual periodicity was found over the most of the area, but even longer periodicities were identified from latitude 37°S in direction NE, alongshore of Uruguay to Brazil, possibly related to discharge fluctuations of Rio de la Plata associated with the El Niño phenomena. The analysis of pixel gradient distribution reveals increased phytoplankton abundance corresponding to the saline front of the estuarine system of Rio de la Plata, and to the strip of the platform that extends along the isobaths of 80 m (coast of Uruguay), especially in the center and south of the study area. Our findings, obtained by using robust statistical methods could contribute to deepen our comprehension of the complex biophysical processes that govern the space-time dynamics of the variability of Chlorophyll-*a* data within the BMCZ.

Acknowledgements

Two anonymous referees are acknowledged for their constructive review. Moderate Resolution Imaging Spectrophotometer (MODIS) data were distributed by the NASA Ocean Biology Processing Group (http://oceancolor.gsfc.nasa.gov/). This study was partially funded by Mincyt-MAE Project 1302.

References

Acha, E.M., Mianzan, H.W., Guerrero, R.A., Favero, M., Bava, J., 2004. Marine fronts at the continental shelves of austral South America, physical and ecological processes. J. Mar. Syst. 44 (1—2), 83—105, http://dx.doi.org/10.1016/j.jmarsys.2003.09.005.

Acha, M., Mianzan, H., Guerrero, R., Carreto, J., Giberto, D., Montoya, N., Carignan, M., 2008. An overview of physical and ecological processes in the Rio de la Plata Estuary. Cont. Shelf Res. 28 (13), 1579—1588, http://dx.doi.org/10.1016/j.csr.2007.01.031.

Ahdesmäki, M., Lähdesmäki, H., Pearson, R., Huttunen, H., Yli-Harja, O., 2005. Robust detection of periodic time series measured from biological systems. BMC Bioinform. 6, 117, http://dx.doi.org/10.1186/1471-2105-6-117 18 pp.

Brandini, F., Boltovskoy, D., Piola, A., Kocmur, S., Rottgers, R., Abreu, P.C., Lopes, R., 2000. Multiannual trends in fronts and distribution of nutrients and chlorophyll in the southwestern Atlantic (30-23S). Deep-Sea Res. Pt. I 47 (6), 1015—1033, http://dx.doi.org/10.1016/S0967-0637(99)00075-8.

Braga, E., Chiozzini, V.C., Glaucia, B.B., Maluf, J.C.C., Aguiar, V.M. C., Charo, M., Molina, D., Romero, S.I., Eichler, B.B., 2008. Nutrient distributions over the Southwestern South Atlantic continental shelf from Mar del Plata (Argentina) to Itajaí (Brazil): winter—summer aspects. Cont. Shelf Res. 28 (13), 1649—1661, http://dx.doi.org/10.1016/j.csr.2007.06.018.

Calliari, D., Gomez, N., 2005. Biomass and composition of the phytoplankton in the Río de la Plata: large-scale distribution and relationship with environmental variables during a spring cruise. Cont. Shelf Res. 25 (2), 197—210, http://dx.doi.org/10.1016/j.csr.2004.09.009.

Campos, J.D., Lentini, C.A., Miller, J.L., Piola, A.R., 1999. Interannual variability of the Sea Surface Temperature in the South Brazilian Bight. Geophys. Res. Lett. 26 (14), 2061—2064, http://dx.doi.org/10.1029/1999GL900297.

Carreto, J.I., Lutz, V.A., Carignan, M.O., Colleoni, A.D.C., Marcos, S.G. D., 1995. Hydrography and chlorophyll *a* in a transect from the coast to the shelf-break in the Argentinian Sea. Cont. Shelf Res. 15 (2—3), 315—336, http://dx.doi.org/10.1016/0278-4343(94)E0001-3.

Day Jr., J.W., Hall, C.A.S., Kemp, W.M., Yáñez-Arancibia, A., 1989. Estuarine Ecology. Wiley, New York, 576 pp.

Depetris, P.J., Kempe, S., 1990. The impact of the El Niño 1982 event on the Parana River, its discharge and carbon transport. Palaeogeogr. Palaeocl. 89 (3), 239—244, http://dx.doi.org/10.1016/0921-8181(90)90019-9.

Depetris, P., Kempe, S., Latif, M., Mook, W., 1996. ENSO-controlled flooding in the Paranti River (1904—1991). Naturwissenschaften 83 (3), 127—129, http://dx.doi.org/10.1007/BF01142177.

Framiñan, M., Brown, O., 1986. Study of the Rio de la Plata turbidity front. Part I: spatial and temporal distribution. Cont. Shelf Res. 16 (10), 1259—1283, http://dx.doi.org/10.1016/0278-4343(95)00071-2.

Garcia, C., Garcia, V.T., 2008. Variability of chlorophyll-*a* from ocean color images in the La Plata continental shelf region. Cont. Shelf Res. 28 (13), 1568—1578, http://dx.doi.org/10.1016/j.csr.2007.08.010.

Gonzalez-Silvera, A., Santamaria del Angel, E., Millan-Nuñez, R., 2006. Spatial and temporal variability of the Brazil-Malvinas Confluence and the La Plata Plume as seen by SeaWiFS and AVHRR imagery. J. Geophys. Res. 111, C06010, http://dx.doi.org/10.1029/2004JC002745.

Gordon, A., 1989. Brazil-Malvinas confluence — 1984. Deep-Sea Res. Pt. A 36 (3), 359—384, http://dx.doi.org/10.1016/0198-0149(89)90042-3.

Guerrero, R.A., Acha, E.M., Framiñan, M.B., Lasta, C.A., 1997. Physical oceanography of the Río de la Plata estuary, Argentina. Cont. Shelf Res. 17 (7), 727—742, http://dx.doi.org/10.1016/S0278-4343(96)00061-1.

Huret, M., Dadou, I., Dumas, F., Lazure, P., Garçon, V., 2005. Coupling physical and biogeochemical processes in the Río de la Plata plume. Cont. Shelf Res. 25 (5—6), 629—653, http://dx.doi.org/10.1016/j.csr.2004.10.003.

Lasta, C., Gagliardini, D., Milovich, J., Acha, E., 1996. Seasonal variation observed in surface water temperature of Samborombón Bay, Argentina, using NOAA-AVHRR and field data. J. Coast. Res. 12 (1), 18—25.

Lutz, V., Segura, V., Dogliotti, A., Gagliardini, D., Bianchi, A., Balestrini, C., 2010. Primary production in the Argentine Sea during spring estimated by field and satellite models. J. Plankton Res. 32 (2), 181—195, http://dx.doi.org/10.1093/plankt/fbp117.

Machado, I., Barreiro, M., Calliari, D., 2013. Variability of chlorophyll-*a* in the Southwestern Atlantic from satellite images: seasonal cycle and ENSO influences. Cont. Shelf Res. 53, 102—109, http://dx.doi.org/10.1016/j.csr.2012.11.014.

Marrari, M., Piola, A., Valla, D., Wilding, J., 2016. Trends and variability in extended ocean color time series in the main reproductive area of the Argentine hake, *Merluccius hubbsi* (Southwestern Atlantic Ocean). Remote Sens. Environ. 177, 1—12, http://dx.doi.org/10.1016/j.rse.2016.02.011.

Martinez, A., Ortega, L., 2015. Delimitation of domains in the external Río de la Plata estuary, involving phytoplanktonic and hydrographic variables. Braz. J. Oceanogr. 63 (3), 217—227, http://dx.doi.org/10.1590/S1679-87592015086106303.

Mechoso, C.R., Iribarren, G.P., 1992. Streamflow in southeastern South America and the southern oscillation. J. Climate 5, 1535—1539, http://dx.doi.org/10.1175/1520-0442(1992)005<1535:SISSAA>2.0.CO;2.

Nagy, G., Lopez Laborde, J., Anastasia, L., 1987. Caracterización de ambientes en el Río de la Plata exterior (salinidad y turbiedad óptica). Investigación Oceanol. 1 (1), 31—56.

Pierini, J.O., Lovallo, M., Gómez, E.A., Telesca, L., 2016. Fisher-Shannon analysis of the time variability of remotely sensed sea surface temperature at the Brazil-Malvinas Confluence. Oceanologia 58, 187—195.

Piola, A.R., Campos, E.J., Moller Jr., O., Charo, M., Martinez, C.M., 2000. Subtropical shelf front off eastern South America. J. Geophys. Res. 105 (C3), 6566—6578, http://dx.doi.org/10.1029/1999JC000300.

Piola, A.R., Matano, R., Palma, E., Moller Jr., O., Campos, E., 2005. The influence of the Plata River discharge on the western South Atlantic shelf. Geophys. Res. Lett. 32 (1), 1603—1606, http://dx.doi.org/10.1029/2004GL021638.

Piola, A., Martinez, N., Guerrero, R., Jardón, F., Palma, E., Romero, S., 2010. Malvinas-slope water intrusions on the northern Patagonia continental shelf. Ocean Sci. 6, 345—359, http://dx.doi.org/10.5194/os-6-345-2010.

Piola, A., Romero, S., Zajaczkovski, U., 2008. Space time variability of the Plata plume inferred from ocean color. Cont. Shelf Res. 28 (13), 1556—1567, http://dx.doi.org/10.1016/J. Csr.2007.02.013.

Priestley, M., 1981. Spectral Analysis and Time Series, Two-Volume Set, Volume 1-2. Elsevier.

Romero, S., Piola, A., Charo, M., Garcia, C.A.E., 2006. Chlorophyll-*a* variability off Patagonia based on SeaWiFS data. J. Geophys. Res. 111 (C5), 1—11, http://dx.doi.org/10.1029/2005JC003244.

Saraceno, M., Provost, C., Piola, A., 2005. On the relationship between satellite retrieved surface temperature fronts and chlorophyll-*a* in the Western South Atlantic. J. Geophys. Res. 110 (C11), http://dx.doi.org/10.1029/2004JC002736.

Simionato, C., Dragani, W., Meccia, V., Nuñez, M., 2004. A numerical study of the barotropic circulation of the Río de la Plata estuary: sensitivity to bathymetry, the Earth's rotation and low frequency wind variability. Estuar. Coast. Shelf Sci. 61 (2), 261—273, http://dx.doi.org/10.1016/j.ecss.2004.05.005.

Simionato, C., Vera, C., Siegismund, F., 2005. Surface wind variability on seasonal and interannual scales over Río de la Plata Area.

J. Coast. Res. 21 (4), 770—783, http://dx.doi.org/10.2112/008-NIS.1.

Sathicq, M., Bauer, D., Gomez, N., 2015. Influence of El Nino Southern Oscillation phenomenon on coastal phytoplankton in a mixohaline ecosystem on the southeastern of South America: Rio de la Plata estuary. Mar. Pollut. Bull. 98 (1—2), 26—33, http://dx.doi.org/10.1016/j.marpolbul.2015.07.017.

Wichert, S., Fokianos, K., Strimmer, K., 2004. Identifying periodically expressed transcripts in microarray time series data. Bioinformatics 20 (1), 5—20.